Infrared reflectivity study of the phase transitions in sodium ammonium sulfate dihydrate

2006 J. Phys.: Condens. Matter 18 7761

(http://iopscience.iop.org/0953-8984/18/32/023)

INSTITUTE OF PHYSICS PUBLISHING JOURNAL OF PHYSICS: CONDENSED MATTER

J. Phys.: Condens. Matter **18** (2006) 7761–7778 doi:10.1088/0953-8984/18/32/023

Infrared reflectivity study of the phase transitions in sodium ammonium sulfate dihydrate

J L Ribeiro[1], L G Vieira[1], I Tarroso Gomes[1], J Agostinho Moreira[2], A Almeida[2], M R Chaves[2], M L Santos[2] and P P Alferes[2]

[1] Grupo FCD-Centro de Física da Universidade do Minho, Campus de Gualtar, 4710-057 Braga, Portugal
[2] Departamento de Física da Faculdade de Ciências, IFIMUP, Universidade do Porto, Rua do Campo Alegre 687, 4169-007 Porto, Portugal

E-mail: jlr@fisica.uminho.pt

Received 28 April 2006
Published 31 July 2006
Online at stacks.iop.org/JPhysCM/18/7761

Abstract

This work reports a detailed infrared reflectivity investigation of the phase transitions in single crystals of sodium ammonium sulfate dihydrate (SASD). The polarized reflectivity spectra allow us to follow the temperature dependence of the polar vibrational modes and detect the critical behaviour of the vibrational parameters through the two low temperature structural phase transitions observed in the compound. The results obtained show that the mechanism of the transitions in SASD is complex, involving a strong coupling between pseudo-spins and phonons. In the paraelectric phase, the driving mechanism of the first phase transition ($T_{c1} = 95$ K) appears to be related to a relaxation with a characteristic frequency that is much lower than the phonon frequencies. In the temperature range corresponding to the first ferroelectric phase ($T_{c1} > T > T_{c2} = 79$ K), the dynamics of the lattice change considerably and the parameters characterizing several vibrational modes display anomalous temperature dependences. The second phase transition occurring at T_{c2} is marked by an important and discontinuous change of the spectral shape, indicating that a considerable lattice distortion is involved.

(Some figures in this article are in colour only in the electronic version)

1. Introduction

A ferroelectric phase transition is usually considered to be either of the displacive or order–disorder type according to the microscopic mechanism that is involved. A displacive transition stems from a lattice instability originating from the softening of a low frequency phonon mode, whose frequency typically lies in the far infrared region [1]. On the other hand, an order–disorder transition consists of a critical slowing down of a dielectric relaxation below optical

phonon frequencies, usually in the microwave region [2]. This relaxation is caused by the dynamical hopping of disordered ions among several closely spaced sites in the unit cell.

During the last few years, experimental evidence has made progressively clear that this distinction is, to some extent, artificial because features of both classes frequently appear simultaneously in a given material [3]. For example, it was recognized early on that pure protonic models, i.e. the ordering of protons in the H-bonds, are not sufficient to explain the ferroelectric properties of KDP-type ferroelectrics [4]. *Ab initio* calculations have shown that the motion of heavy atoms coupled to protons or deuterons must be taken into account to obtain more realistic descriptions of the phase transition [5]. Following these lines, a strong dipole–proton coupling model (SDPC) has been proposed for these systems [6, 7]. This model suggests, as one example, that protons adiabatically follow the dynamics of the PO_4 dipoles aligned along the *c*-axis, without tunnelling motion. Also, typically order–disorder features have been seen in materials previously recognized as displacive prototypes [8].

The importance of the coexistence and coupling between different mechanisms in a structural phase transition is not unexpected. Displacive and order–disorder types of transition must be considered as limiting cases described by ideal self-consistent phonon and spin-like models, respectively [9]. In real materials, some intermediate and more complex behaviour is expected as a result of specific interactions between the different structural units, and combined experimental studies are necessary to help characterize the role played by different mechanisms. Vibrational spectroscopic studies, by indicating the presence of soft modes or by characterizing the coupling between relaxational pseudo-spins and phonons, may directly clarify the role of lattice dynamics in a given structural phase transition. To a smaller extent, they may also give evidence for relaxational central modes directly related to an order–disorder mechanism.

Similar to the case of the KDP family, a number of ferroelectric materials contain tetrahedral molecular groups like NH_4^+, SO_4^{2-}, SeO_4^{2-}, PO_4^{3-} or AsO_4^{3-}, whose dynamics play an important role in the ferroelectric transition. Among these compounds are the ferroelectric sulfates of the $(NH_4)_2SO_4$ family, which have been known since 1950 [10–20]. Sodium ammonium sulfate dihydrate (SASD) or lecontite, $NaNH_4SO_4{\cdot}2H_2O$ [21], together with its isomorphic compound $NaNH_4SeO_4{\cdot}2H_2O$ (SASeD) [22], are hydrated compounds of this family of polar materials. They present a variety of chemical bonds, including hydrogen bonds, which may potentially play a role in the ferroelectric transition.

The similar structures displayed by these two compounds in the paraelectric phase (enantiomorphic non-polar space group $P2_12_12_1$, $z = 4$) and the strong correlation between the observed values of the critical temperatures ($T_c = 101$ K and $T_c = 180$ K in SASD and SASeD, respectively) and the molecular masses of the SO_4 and SeO_4 groups, indicate a similar driving mechanism for the structural transitions. This mechanism has been viewed as resulting from an order–disorder process of the sulfate (or selenate) groups [23] and described on the basis of the Mitsui model [23–25]. The Mitsui model, first introduced to explain the ferroelectric phase of the Rochelle salt [26], requires two types of active molecular groups in a two sub-lattice system. In SASD [or SASeD], these two sub-lattices would be formed by the SO_4(I) [SeO_4(I)] and the SO_4(II) [SeO_4(II)] groups which, in the paraelectric phase, are symmetrically equivalent but oppositely oriented so that the total polarization in each unit cell vanishes (see below for details of the crystal structure).

However, there are also striking differences between the two compounds that are often overlooked. One difference is the existence, in SASD but not in SASeD, of two distinct dielectric anomalies that mark two structural transformations (at $T_{c1} = 101$ K and $T_{c2} = 92$ K [11]). A second difference is the order of magnitude of the electrical polarization and dielectric constant. In fact, the dielectric constant (along the polar axis) near the phase transitions and the saturation value of the polarization are of the order of 700 and 2 μC cm^{-2}

in SASeD, and only 40 and 6 nC cm^{-2} in SASD, respectively [11, 22, 27]. In addition, the structure of the ferroelectric phase is known for SASeD (monoclinic, $P2_1$ space group [22]) but not for SASD.

These differences could signal that separate mechanisms may be responsible for the structural transformation in the two compounds. The wealth of chemical bonds present in the crystal structure of SASD, along with the peculiar existence of two dielectric anomalies, suggests that one may likely have to go beyond the simple approximation of an order–disorder model in order to fully understand the mechanism of the phase transitions in SASD. Even in the case of SASeD, there is evidence for other contributions beyond the ordering process of the SeO_4 groups [22]. These include other order–disorder processes, such as the ordering of hydrogen bonds, together with additional distortions of the SeO_4 groups and the interaction of SeO_4 and H_2O vibrations.

In the present work, we report a detailed investigation of the infrared reflectivity of SASD over the range of temperatures that corresponds to the observed phase transitions. Infrared spectroscopy allows us to follow the temperature dependence of the polar vibrational modes directly and detect the critical behaviour of the parameters of the polar modes across the para–ferroelectric phase transition. To date, there has been no detailed IR spectroscopic investigation of SASD. To the best of our knowledge, only Acharya and Narayanan [28] have published non-polarized infrared transmission spectra of SASD, taken in a mujol mull in the spectral range 250–3500 cm^{-1}, at room temperature and at 110 K. Hence, this study does not relate to the investigation of the phase transitions (since both temperatures are above T_{c1}), nor provide information on the behaviour of the lattice modes.

The study of temperature dependence of the reflectivity spectra allows us to observe the critical anomalies displayed by the vibrational parameters of the different molecular units. They confirm that the phase transitions in SASD are complex and involve a strong coupling between the SO_4 pseudo-spins and the lattice. In agreement with dielectric measurements, they also provide clear spectroscopic evidence for the existence of an intermediate phase, occurring in a narrow temperature range between the paraelectric and the lower temperature ferroelectric phase.

2. Experimental details

Colourless crystals of SASD were grown at 40 °C by slow evaporation from aqueous solutions of the constituents with equimolar ratio of Na_2SO_4 and $(NH_4)_2SO_4$. The crystal used measured about 3 cm and contained large areas of optical quality.

IR reflectivity measurements were performed with a Bruker IFS 66 V spectrometer. Room temperature pyroelectric detectors of DTGS with PE or KBr windows and Mylar 6μ-M8 or KBr beam-splitters were used to cover the spectral range 40–4000 cm^{-1}. The complex dielectric function has been evaluated from the IR data both by Kramers–Kronig inversion and by fitting the factorized form of the dielectric function [29],

$$\varepsilon(\omega) = \varepsilon_\infty \prod_{j=1}^{N} \frac{\Omega_{j\mathrm{LO}}^2 - \omega^2 - \mathrm{i}\omega\gamma_{j\mathrm{LO}}}{\Omega_{j\mathrm{TO}}^2 - \omega^2 - \mathrm{i}\omega\gamma_{j\mathrm{TO}}}, \tag{1}$$

to the reflectivity spectra at normal incidence, via

$$R(\omega) = \left| \frac{\sqrt{\varepsilon(\omega)} - 1}{\sqrt{\varepsilon(\omega)} + 1} \right|^2. \tag{2}$$

In equation (1), $\Omega_{j\mathrm{TO(LO)}}$ and $\gamma_{j\mathrm{TO(LO)}}$ represent the frequency and damping coefficient of the jth transversal (longitudinal) optical mode, and ε_∞ the electronic contribution to the

dielectric constant. From the fitting, the oscillator strength $\Delta\varepsilon_j$ of each mode can be evaluated as

$$\Delta\varepsilon_j = \frac{\varepsilon_\infty}{\Omega^2_{j\mathrm{TO}}} \frac{\prod_{k=1}^{N}\left(\Omega^2_{k\mathrm{LO}} - \Omega^2_{j\mathrm{TO}}\right)}{\prod_{k\neq j}^{N}\left(\Omega^2_{k\mathrm{TO}} - \Omega^2_{j\mathrm{TO}}\right)}. \tag{3}$$

We have imposed the condition of equal damping coefficients for longitudinal and transversal optical modes ($\gamma_{j\mathrm{TO}} = \gamma_{j\mathrm{LO}} = \gamma_j$). Under such a condition, the factorized form (1) corresponds to the conventional sum of polar Lorentz oscillators.

Because the crystal dehydrates easily, the measurements were made with the sample mounted in a cryostat kept at ambient pressure. The reference for the reflectivity was made at each temperature. The rate of change of the temperature was kept below 1 K min^{-1}. The measurements were made isothermically (stability better than 0.1 K) after a stabilization period of about 20 min.

3. Experimental results

3.1. The infrared spectra at room temperature

As referred to in the preceding section, the crystal structure of SASD is known only for the paraelectric phase. According to the available crystallographic data [15], the unit cell of the paraelectric phase is orthorhombic, with space group $P2_12_12_1$ and four molecules per unit cell ($Z = 4$). The lattice parameters are $a = 8.24$, $b = 12.91$ and $c = 6.27$ Å. In the ferroelectric phase, the spontaneous polarization is parallel to the c-axis.

Figure 1 shows the ORTEP [30] plot of the crystal structure at room temperature. The backbone structure can be regarded as made of chains or columns of NaO_6 octahedra, sharing three oxygen atoms on a face, approximately aligned along the c-axis. Four of the six oxygen atoms in one octahedron come from the crystal water and two come from two sulfate groups SO_4. These NaO_6 chains are well separated and do not share common SO_4 tetrahedra. They are interlaced with chains of NH_4–SO_4–NH_4. The two types of chain are linked by sharing one oxygen from the SO_4 tetrahedron and by hydrogen bonds.

In the unit cell (factor group D_2), each atom or molecular group is placed at a site with general symmetry (C_1) and the asymmetric unit contains 17 atoms. Consequently, site symmetry analysis [31] indicates the following decomposition for the normal modes at the centre of the Brillouin zone:

$$51\mathrm{A} + 50\mathrm{B}_1 + 50\mathrm{B}_2 + 50\mathrm{B}_3.$$

The A modes are Raman active and the B_1, B_2 and B_3 modes are Raman and IR active.

If we consider five molecular groups (Na–NH_4–SO_4–H_2O–H_2O) as rigid units, placed at sites of symmetry C_1 and take into account that the Na atoms cannot have rotational degrees of freedom, we obtain $15\mathrm{A} + 14\mathrm{B}_1 + 14\mathrm{B}_2 + 14\mathrm{B}_3$ and $12\mathrm{A} + 12\mathrm{B}_1 + 12\mathrm{B}_2 + 12\mathrm{B}_3$ external translational and rotational (librational) modes, respectively.

Table 1 shows the correlation between the vibrations of the free molecular units (water, ammonium and sulfate) and the corresponding internal modes in the paraelectric phase. As shown, for each polar symmetry (B_1, B_2 and B_3) one may in principle detect the 24 internal modes ($6 + 9 + 9$) of the water, ammonium and sulfate groups.

On another hand, a free tetrahedral ion AB_4 has nine vibration modes (ν_1 (symmetric), ν_2 (silent, double degenerated), ν_3 and ν_4, both triply degenerate). In the orthorhombic structure, such an ion cannot retain the cubic symmetry and the highest symmetry it can possess is a

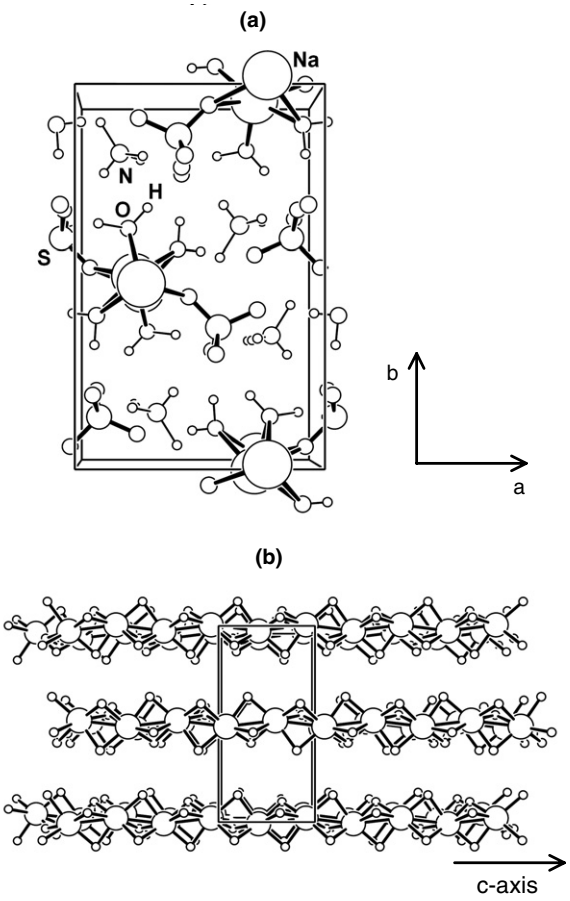

Figure 1. The ORTEP plot (Ortep-3 for Windows, [30]) of the crystal structure of SASD at room temperature: (a) the unit cell projected on the [001] direction; (b) the NaO_6 columns directed along the *c*-axis. The crystallographic data were taken from [21].

mirror symmetry. Consequently, all the degenerate modes split, giving rise to nine modes that can be detected either by Raman or IR measurements (at any polarization). In a crystal, combinations and overtones may also occur.

A free molecule of water (symmetry C_{2v}) has three non-degenerate normal modes of vibration (ν_1 (symmetric stretching), ν_2 (bending) and ν_3 (asymmetric stretching)). In a crystal, the three rotational degrees of freedom per molecule may give rise to detectable librational modes. These librational modes occur in the frequency range 400–800 cm^{-1}. The frequencies at which the different modes of the free ions are observed are listed in table 2.

Let us now consider the infrared spectra measured in the paraelectric phase of SASD. Figure 2 shows the polarized reflectivity spectra taken at ($T = 250$ K) (circles) in the spectral range 40–3500 cm^{-1}, for polarizations $\vec{E} \parallel \vec{a}$ (symmetry B_3), $\vec{E} \parallel \vec{b}$ (symmetry B_2) and $\vec{E} \parallel \vec{c}$ (symmetry B_1), together with the curves fitted with the factorized form of dielectric function (lines). The frequency dependence of the complex dielectric functions can thus be obtained from the reflectivity data via equation (1) for the three geometries considered. The parameters corresponding to the best fits are listed in table 3, together with the assigned origin of the modes.

Table 1. Correlation between the molecular vibration and internal modes in SASD.

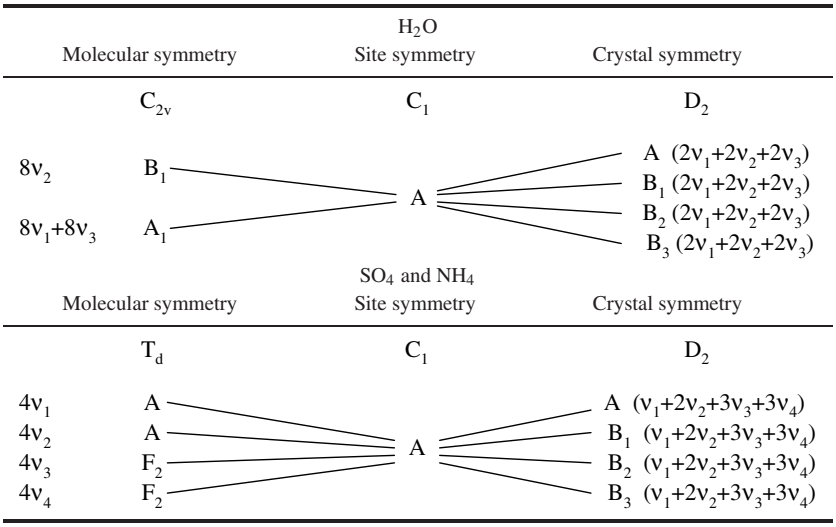

Table 2. Frequencies of the vibrational modes in the free molecular units.

(C_{2v})	Free molecule	ν_1	ν_2	ν_3	
	H_2O	3657 cm^{-1}	1595 cm^{-1}	3756 cm^{-1}	
	Symmetry	(A_1)	(B_1)	(A_1)	
	Degeneracy	1	1	1	
(T_d)	Free ion	ν_1	ν_2	ν_3	ν_4
	NH_4	3033 cm^{-1}	1685 cm^{-1}	3134 cm^{-1}	1397 cm^{-1}
	SO_4	981 cm^{-1}	451 cm^{-1}	1104 cm^{-1}	613 cm^{-1}
	Symmetry	(A_1)	(E)	(F_2)	(F_2)
	Degeneracy	1	2	3	4

From these data it can be seen that one can deduce the origin of the majority of the detected internal modes simply by taking into account the frequencies listed for the free ions or molecules. We have also taken into account the previous analyses of IR spectra of powdered samples by Acharya *et al* [28] and Raman data by Fawcett *et al* [32]. In general, with the exception of the modes related to hindered rotations of the tetrahedral groups, we found a good agreement between our data and the results reported by these authors. In fact, the rotational degrees of freedom of a molecular group may give rise, in a crystal, to rotational modes. In the case of a tetrahedral group, these modes, designated as ν_6 modes, can eventually combine with the ν_2 and ν_4 modes to give rise to combinational modes $\nu_6 + \nu_2$ and $\nu_6 + \nu_4$ [33]. Acharya *et al* [28] identified two ν_6 modes of the NH_4 located at 255 and 310 cm^{-1}, along with a combinational $\nu_6 + \nu_2$ mode at 2070 cm^{-1}. We were not able to detect evidence for these modes in the reflectivity data.

We could detect 18 external modes with frequencies below 400 cm^{-1}, that result from external vibrations (including the Na–O stretching modes). As referred to above, symmetry would allow up to 23 modes for each polarization. A strong mode mixing, a partial overlap of the external mode frequencies or the weak effective charges of some modes may be at the origin of this fact. It is difficult to identify the origin of the external modes detected. According

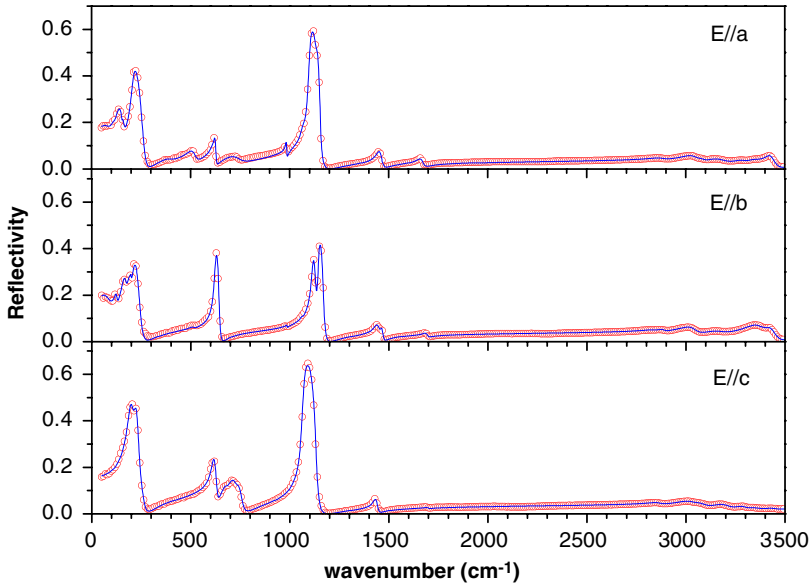

Figure 2. Reflectivity spectra measured at 250 K for the three geometries (circles) and the curves fitted with the factorized form of the dielectric function (lines). For clarity not all experimental points are plotted.

to literature [34], librations and translation modes of the SO_4 ion are usually located at about 75–80 cm^{-1}, 95–105 cm^{-1} and 169–175 cm^{-1}. External modes related to the ammonium group are typically found at the frequencies 165–170 cm^{-1} and 394 cm^{-1}.

Let us consider now the internal modes of the SO_4 ion. Only two ν_4 modes are found at the wavenumbers 615 cm^{-1} ($\vec{E} \parallel \vec{c}$ and $\vec{E} \parallel \vec{b}$) and 622 cm^{-1} ($\vec{E} \parallel \vec{c}$ and $\vec{E} \parallel \vec{a}$) whose frequencies are independent of the polarization employed. Remember that symmetry would allow for a complete splitting of the mode into three different frequencies. The symmetric mode ν_1, which is IR inactive in the free ion, could be detected with the $\vec{E} \parallel \vec{c}$ and $\vec{E} \parallel \vec{a}$ geometries at 984 cm^{-1}. Finally, the ν_3 modes were located in the wavenumber range 1066–1143 cm^{-1}. Evidence of the complete removal of degeneracy of this mode could be found only using the $\vec{E} \parallel \vec{a}$ geometry. These results concerning the internal modes of the SO_4 ion indicate that the anion loses its tetrahedral symmetry (as expected from symmetry considerations). Also, consistent with the space group of the paraelectric phase, the four SO_4 ions in the unit cell are spectroscopically equivalent.

In the free ion, the mode ν_2 of the SO_4 group is not IR active and it has the lowest frequency (465 cm^{-1}) among the internal modes of the ion. In an orthorhombic crystal, this mode may become active due to a symmetry breaking caused by the crystal field. Contrary to the results in [28], we could not detect any mode in the frequency range expected for such a mode.

As with the sulfate group, the lifting of degeneracy of the ν_4 mode of NH_4 could only be detected with the $\vec{E} \parallel \vec{a}$ geometry (1434–1465 cm^{-1}). In the case of the ν_2 mode, located in the range 1666–1699 cm^{-1}, the lifting of degeneracy could not be resolved. For the ν_3 modes, a splitting into three different frequencies for $\vec{E} \parallel \vec{b}$ and $\vec{E} \parallel \vec{c}$ could be detected.

At a higher spectral range, the stretching modes of the water could be detected between 3354–3449 cm^{-1}. At 514 cm^{-1} and in the frequency range 674–744 cm^{-1}, we can detect several modes that originate from internal librational oscillations of the water molecules.

Table 3. Parameters corresponding to the best fit of the factorized dielectric function to the reflectivity spectra taken at 78 K (FE-2), 80 K (FE-1) and 250 K (PE-phase).

$T = 78$ K				$T = 80$ K				$T = 250$ K				
Ω_{TO} (cm^{-1})	γ_{TO} (cm^{-1})	TO strength	Pol.	Ω_{TO} (cm^{-1})	γ_{TO} (cm^{-1})	TO strength	Pol.	Ω_{TO} (cm^{-1})	γ_{TO} (cm^{-1})	TO strength	Pol.	Mode assignment
70	14	0.1555	a	73	7	0.1191	a	67	4	0.0117	a	External
90	21	0.2741	c	90	21	0.2941	c	81	52	0.5498	c	Modes
98	12	0.2161	a	93	15	0.2679	a	83	67	1.6673	a	
123	15	0.1146	c	123	42	0.1237	c	112	7	0.0112	c	
135	10	0.1302	a	132	8	0.1198	a	125	16	0.2008	a	
153	7	0.7273	c	153	14	0.7559	c	146	36	1.1593	c	
165	10	0.1228	c	166	8	0.1218	c	155	8	0.0318	c	
167	7	0.2486	b	169	11	0.4327	a	164	33	0.9449	a	
171	9	0.2083	a	178	18	0.5824	b	174	33	0.4939	b	
178	10	0.7039	b	179	12	0.3548	a	188	20	0.2222	a	
183	8	0.1047	c	192	21	0.4535	c	190	28	1.6810	b	
184	7	0.2207	a	195	16	1.4384	b	197	9	0.0487	a	
195	11	0.5381	a	199	18	0.7860	a	206	33	0.5851	a	
198	10	0.2212	c	215	16	0.8786	c	209	31	1.3464	c	
202	9	0.8016	b	220	13	0.3333	a	215	27	0.2272	b	
210	7	0.3109	a	220	16	0.3968	b	220	35	0.0059	c	
215	10	0.4009	b	231	20	0.0362	c	242	41	0.0318	b	
220	10	0.6307	c	243	33	0.0156	b	394	84	0.0656	c	
220	9	0.3191	a	377	23	0.0126	a					
240	13	0.1272	c	398	50	0.0439	c					
251	10	0.0476	b									
377	23	0.0128	a									
397	50	0.0470	c									
503	10	0.0661	c	529	25	0.0760	c	514	47	0.0923	c	Libration
550	10	0.0442	c	535	18	0.0097	a	514	25	0.0085	a	H_2O
551	10	0.0122	a									
587	7	0.0090	b	612	6	0.0113	c	615	30	0.0603	c	ν_4 SO_4^{2-}
599	10	0.0101	c	621	14	0.1902	b	616	24	0.1826	b	
612	5	0.0091	c	623	10	0.0532	c	623	15	0.1786	a	
621	14	0.1845	b	627	9	0.2073	a	623	11	0.0124	c	
623	6	0.0500	c									
630	6	0.1366	a									
643	8	0.0655	a									
668	13	0.0178	c	668	13	0.0183	c	674	40	0.0591	b	Libration
686	15	0.1643	b	679	26	0.1066	b	707	59	0.1815	b	H_2O
727	15	0.0617	b	718	37	0.1603	b	731	106	0.0985	c	
743	16	0.0191	c	743	16	0.0194	c	744	39	0.0318	b	
759	15	0.0735	b	749	20	0.0520	b					
984	5	0.0130	c	984	5	0.0131	c	984	6	0.0093	c	ν_1 SO_4^{2-}
984	13	0.0065	a	984	13	0.0065	a	985	6	0.0016	a	
987	5	0.0075	b									
1070	6	0.0202	c	1065	7	0.2731	b	1066	18	0.2586	b	ν_3 SO_4^{2-}
1075	5	0.2549	b	1070	13	0.0050	a	1066	18	0.0030	a	
1099	7	0.2023	c	1070	12	0.0204	c	1073	25	0.0298	c	
1106	5	0.0144	b	1099	8	0.2043	c	1098	17	0.1949	c	
1115	8	0.1652	a	1119	13	0.1373	a	1116	19	0.1338	a	

Table 3. (Continued.)

$T = 78$ K				$T = 80$ K				$T = 250$ K				
Ω_{TO} (cm^{-1})	γ_{TO} (cm^{-1})	TO strength	Pol.	Ω_{TO} (cm^{-1})	γ_{TO} (cm^{-1})	TO strength	Pol.	Ω_{TO} (cm^{-1})	γ_{TO} (cm^{-1})	TO strength	Pol.	Mode assignment
1130	7	0.0032	b	1135	8	0.0002	c	1143	15	0.0405	a	
1135	6	0.0002	c	1141	9	0.0589	a					
1141	8	0.0489	a	1152	9	0.0019	a					ν_3 SO_4^{2-}
1152	8	0.0017	a									
1432	10	0.0115	b	1436	13	0.0196	b	1434	25	0.0215	b	ν_4 NH_4^+
1437	8	0.0020	c	1443	14	0.0188	a	1443	30	0.0234	a	
1444	14	0.0144	a	1450	15	0.0176	c	1454	32	0.0324	c	
1446	10	0.0103	b	1468	12	0.0175	a	1465	17	0.0092	a	
1454	11	0.0175	c	1466	17	0.0096	c					
1463	10	0.0073	b									
1468	10	0.0179	a									
1470	20	0.0107	c									
1658	11	0.0040	c	1671	22	0.0120	c	1666	36	0.0167	c	ν_2 NH_4^+
1674	11	0.0054	c	1698	11	0.0033	a	1692	25	0.0060	a	
1698	11	0.0033	a	1699	13	0.0012	b	1699	20	0.0013	b	
1699	13	0.0007	b									
2350	20	0.0019	c	2358	8	0.0052	a					?
2359	20	0.0041	a	2360	6	0.0024	c					
2360	21	0.0039	b	2370	21	0.0080	b					
2380	20	0.0018	c	2371	17	0.0053	a					
				2375	26	0.0071	c					
2844	53	0.0006	a	2844	23	0.0006	a	2836	65	0.0020	a	$2\nu_4$ NH_4^+
2887	57	0.0031	c	2874	23	0.0024	b	2867	73	0.0047	b	
2895	50	0.0044	a	2887	57	0.0032	c	2882	84	0.0053	c	
2895	80	0.0053	b	2896	31	0.0027	a	2889	43	0.0028	a	
3008	17	0.0036	b	3032	53	0.0083	b	3025	97	0.0112	b	ν_1 NH_4^+
3010	30	0.0059	a	3038	50	0.0211	a	3035	88	0.0191	a	
3020	23	0.0050	c	3042	44	0.0127	c	3041	87	0.0148	c	
3028	13	0.0030	a									
3055	29	0.0035	c	3077	40	0.0122	b	3085	90	0.0105	b	ν_3 NH_4^+
3068	24	0.0031	a	3082	29	0.0057	c	3087	44	0.0021	c	
3077	45	0.0131	b	3153	43	0.0049	c	3169	133	0.0133	a	
3097	17	0.0027	c	3157	22	0.0012	a	3174	137	0.0213	c	
3157	23	0.0012	a	3179	29	0.0034	b	3200	103	0.0137	b	
3165	39	0.0037	c	3234	32	0.0032	a	3287	62	0.0036	c	
3179	40	0.0035	b	3241	42	0.0032	b	3293	56	0.0038	b	
3234	49	0.0030	a	3241	28	0.0015	c					
3235	60	0.0047	b	3289	33	0.0067	c					
3242	50	0.0010	c	3289	27	0.0097	a					
3293	25	0.0058	c	3292	31	0.0111	b					
3292	46	0.0082	a									
3293	31	0.0094	b									
3330	32	0.0157	a	3350	40	0.0034	b	3354	106	0.0067	b	ν_1 H_2O
3332	35	0.0055	c	3353	61	0.0406	a	3357	100	0.0100	c	
3355	40	0.0065	b	3365	59	0.0147	c	3359	108	0.0329	a	
3363	35	0.0088	c									

Table 3. (Continued.)

$T = 78$ K				$T = 80$ K				$T = 250$ K				
Ω_{TO} (cm^{-1})	γ_{TO} (cm^{-1})	TO strength	Pol.	Ω_{TO} (cm^{-1})	γ_{TO} (cm^{-1})	TO strength	Pol.	Ω_{TO} (cm^{-1})	γ_{TO} (cm^{-1})	TO strength	Pol.	Mode assignment
3420	34	0.0221	a	3402	50	0.0258	a	3428	63	0.0188	c	ν_3 H_2O
3433	30	0.0210	c	3419	100	0.0180	b	3428	72	0.0161	a	
3442	30	0.0133	a	3424	32	0.0231	c	3449	84	0.0035	b	
3450	100	0.0171	b									

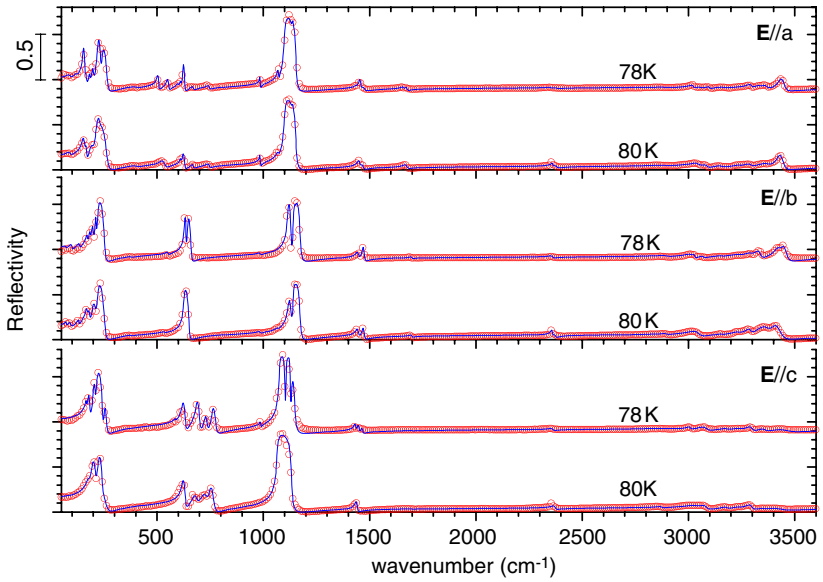

Figure 3. Reflectivity spectra measured at 78 and 80 K for the three geometries (circles) and the curves fitted with the factorized form of the dielectric function (lines). For clarity not all experimental points are plotted.

3.2. Temperature dependence of the spectra

Figure 3 shows the reflectivity spectra registered at the temperatures $T = 80$ and 78 K, together with the curves fitted with the factorized form of the dielectric function. The parameters corresponding to the fitted curves are given in table 3.

The reflectivity spectra of SASD show considerable changes due to temperature effects, especially in the vicinity of the phase transitions. For simplicity, we will focus our attention on the temperature dependence of the imaginary part of the dielectric function (ε_2), and follow the modification observed in the frequency ranges corresponding to the modes of the different molecular units.

The comparison of the spectra taken in the paraelectric phase with those shown in figure 3 allows us to observe several modifications that indicate the occurrence of two phase transitions. As will be shown from the detailed analysis of the temperature dependence of the vibrational parameters, the first transition occurs at $T_{c1} = 95$ K. A second transition, which produces a discontinuous change of the spectra, occurs at $T_{c2} = 79$ K. As referred to above, the existence of two distinct phase transitions in SASD has been previously suggested from the analysis of the

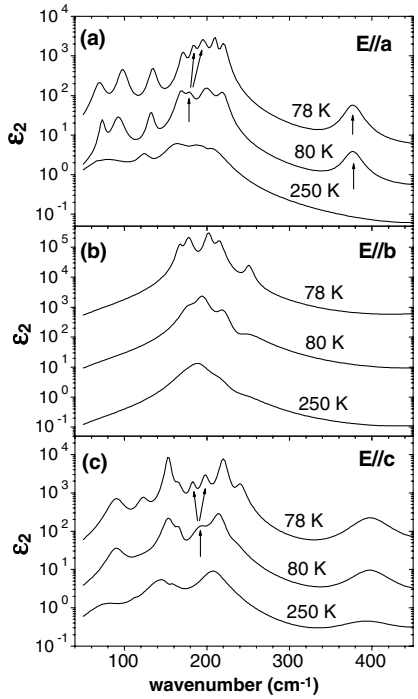

Figure 4. Dispersion of the imaginary part of the dielectric function in the spectral range of the external modes. For each of the geometries considered, the curves shown correspond to the temperatures 78, 80 and 250 K. The arrows indicate the bands referred to in the text.

temperature dependence of the low frequency dielectric constant and polarization. The critical temperatures observed from the reflectivity data are lower than those reported from dielectric measurements ($T_{c1} = 101$ K and $T_{c2} = 92$ K) [11]. However, these latter critical temperatures correspond to samples grown from aqueous solution containing an excess of $(NH_4)_2SO_4$. Crystals grown with this method have a tendency to exhibit higher critical temperatures [11].

3.2.1. Lattice modes. Figure 4 shows the frequency dependence of ε_2 in the spectral range of the external modes. In general, as the temperature decreases, the external modes tend to harden while their damping factors decrease. This behaviour is expected from non-harmonic effects and bears no relation to critical phenomena. However, the comparison between the spectra taken at 250 and 80 K clearly shows the appearance of two additional bands at 191 cm^{-1} ($\vec{E} \parallel \vec{c}$) and 179 cm^{-1} ($\vec{E} \parallel \vec{a}$). On further cooling, these two bands split, giving rise to bands located at 183 and 198 cm^{-1} for $\vec{E} \parallel \vec{c}$ and at 184 and 195 cm^{-1} for $\vec{E} \parallel \vec{a}$. These results clearly suggest that there are two distinct symmetry breaking stages on entering into the lowest temperature ferroelectric phase.

At higher frequencies, we note that the band located at about 380 cm^{-1}, likely due to an external translational mode of the ammonium group, becomes active below T_{c1} for $\vec{E} \parallel \vec{a}$. This activation may therefore indicate a change of the geometry and orientation of the NH_4 groups at the onset of the first polar phase.

For the $\vec{E} \parallel \vec{b}$ spectra we could not detect any anomalous behaviour in the modes located in this spectral range.

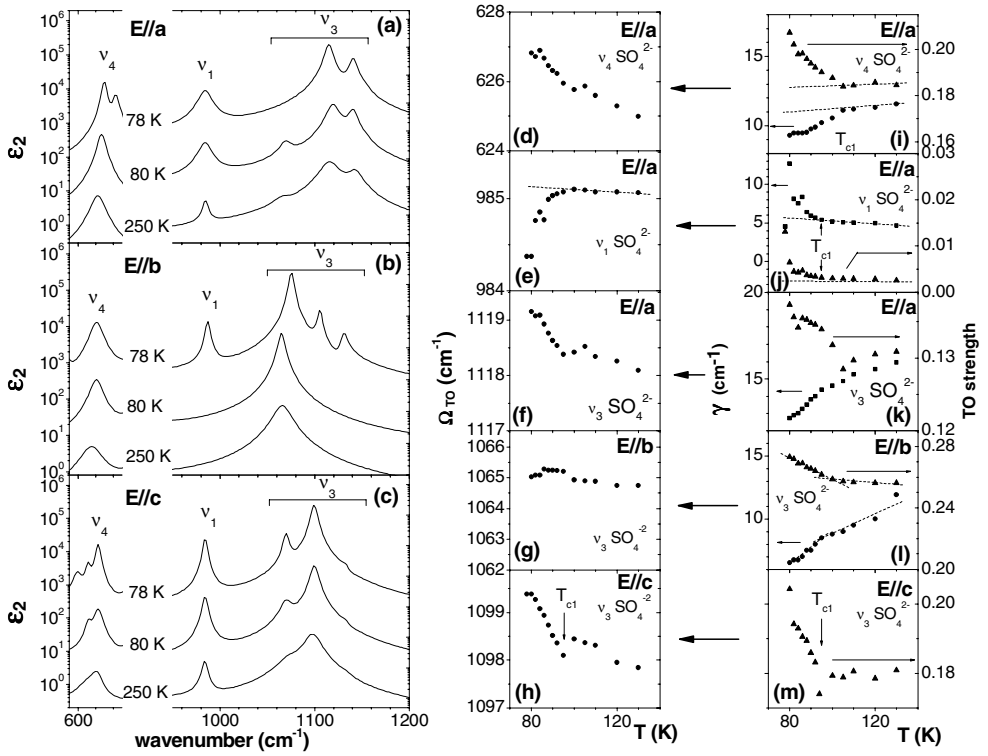

Figure 5. The imaginary part of the dielectric function over the spectral ranges corresponding to the internal modes of SO_4^{2-}. For each of the geometries considered, the curves shown in figures (a)–(c) correspond to the temperatures 78, 80 and 250 K. Figures (d)–(m) display illustrative examples of the temperature dependence of the frequency and damping coefficients of these modes.

3.2.2. SO_4 internal modes. The frequency and temperature dependence of the internal modes of the sulfate ion are illustrated in figure 5. At room temperature, the internal modes of the SO_4 group are detected at 615 and 622 cm^{-1} (ν_4), 984 cm^{-1} (ν_1), 1066–1142 cm^{-1} (ν_3). In the paraelectric phase ($T < T_{c1} = 95$ K), the ν_1 mode is detected only for the $\vec{E} \parallel \vec{a}$ and $\vec{E} \parallel \vec{c}$ geometries (with dielectric strengths of the order of 0.001 and 0.01, respectively). As shown in figure 5(e), the frequency of this mode for $\vec{E} \parallel \vec{a}$ is nearly temperature independent for $T < T_{c1}$. Below T_{c1}, its frequency softens while its dielectric strength and damping increase on approaching $T_{c2} = 79$ K. Below T_{c2}, the ν_1 mode also becomes visible for the $\vec{E} \parallel \vec{b}$ geometry (see figure 5(b)).

In the paraelectric phase, the three ν_3 modes can be well discriminated for $\vec{E} \parallel \vec{a}$ and $\vec{E} \parallel \vec{c}$ but not for $\vec{E} \parallel \vec{b}$, where only a single effective band is seen. As illustrated in figures 5(f)–(h) and (k)–(l), the frequency, strength and damping of these bands display anomalies at T_{c1}. Note however that the magnitude of the changes detected in the TO frequencies of the SO_4 internal modes are rather small, which may indicate that they behave as rigid units across T_{c1}. In contrast, the magnitude of the anomalies detected in the temperature dependence of the dielectric strength and damping parameters are relatively important (see figures 5(f)–(h) and (k)–(m)). Note also that the values of the dipolar strength of the modes ν_3 and ν_4 of the sulfate group are the highest among all the internal modes of the compound.

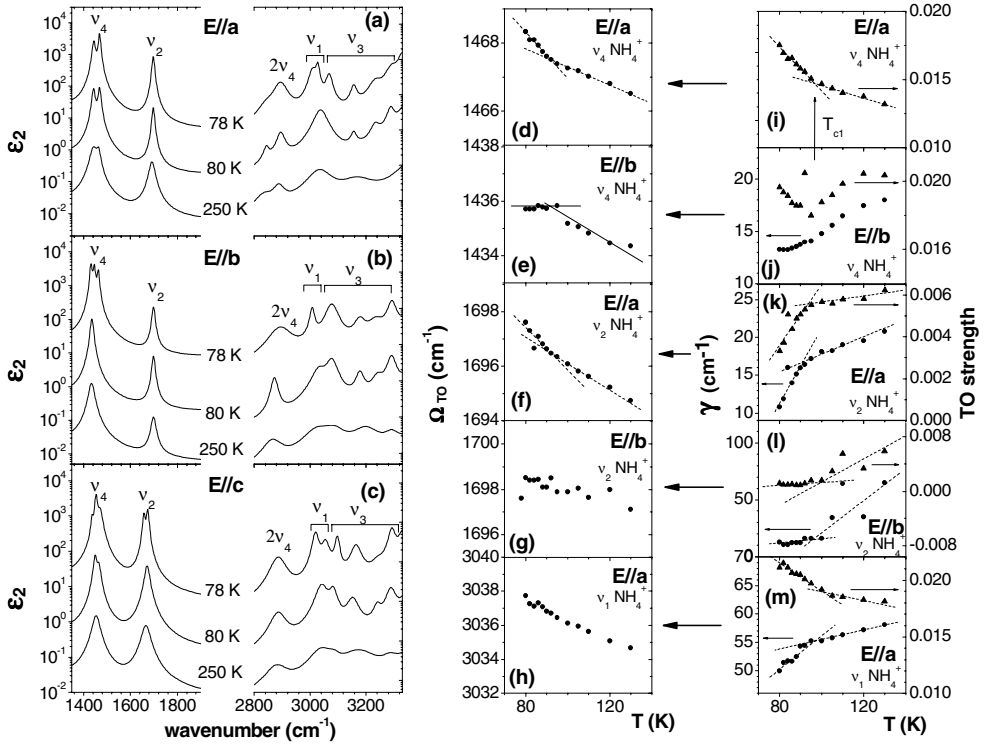

Figure 6. The imaginary part of the dielectric function over the spectral ranges corresponding to the internal modes of NH_4^{2-}. For each of the geometries considered, the curves shown in figures (a)–(c) correspond to the temperatures 78, 80 and 250 K. Figures (d)–(m) display illustrative examples of the temperature dependence of the frequency and damping coefficients of these modes.

The modes ν_3 and ν_4 also clearly reflect the onset of a second transition at T_{c2}. As can be observed in figure 5(a), the lower frequency component of the ν_3 triplet observed for $\vec{E} \parallel \vec{a}$ disappears discontinuously at $T = 78$ K, while for $\vec{E} \parallel \vec{b}$ the three components become clearly resolved. These observations indicate that the deformation of the SO_4 tetrahedra and the orientation of their principal inertial axes are modified at T_{c2}. A similar conclusion can be drawn from the behaviour displayed by the ν_4 mode, as depicted in figure 5(a) ($\vec{E} \parallel \vec{a}$) and 5(c) ($\vec{E} \parallel \vec{c}$).

3.2.3. The NH_4 modes. The dielectric strengths of the internal modes of the ammonium group are relatively modest if compared with those of the sulfate group. In the paraelectric phase, the three components allowed by symmetry for the ν_4 bands (located around 1450 cm^{-1}) could not be fully resolved in any of the geometries considered. As can be seen in figures 6(a)–(c), only single effective modes or a doublet are detected using the $\vec{E} \parallel \vec{c}$ and $\vec{E} \parallel \vec{b}$ or $\vec{E} \parallel \vec{a}$ geometries, respectively. On cooling, the frequencies of these bands increase slightly. At T_{c1}, the temperature derivatives of the frequency, damping and strength change discontinuously (see figures 6(d)–(e) and (i)–(j)) and the effective mode detected using the $\vec{E} \parallel \vec{c}$ geometry splits into a doublet (figure 6(c)). Further cooling induces dramatic changes in the ν_4 bands, particularly for the $\vec{E} \parallel \vec{c}$ and $\vec{E} \parallel \vec{b}$ geometries. As shown in figure 6(b), the effective mode detected for $\vec{E} \parallel \vec{b}$ discontinuously splits into a triplet, while a third ν_4 mode appears for $\vec{E} \parallel \vec{c}$ (figure 6(a)).

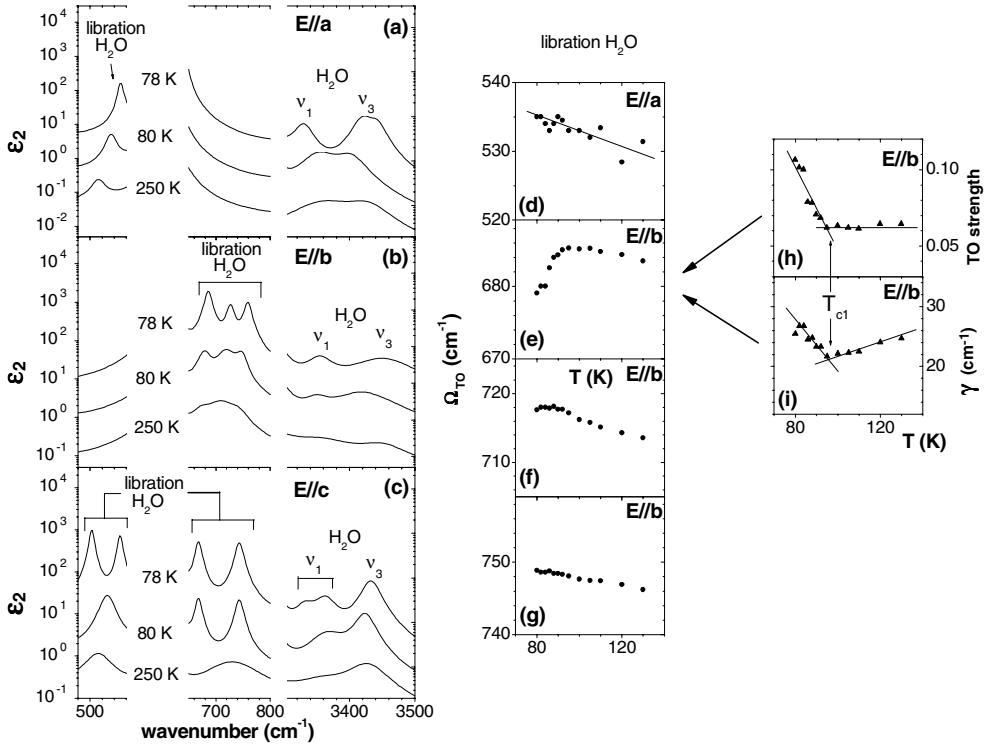

Figure 7. The imaginary part of the dielectric function over the spectral ranges corresponding to the internal modes of the water molecules. For each of the geometries considered, the curves shown in figures (a)–(c) correspond to the temperatures 78, 80 and 250 K. Figures (d)–(i) show the temperature dependence of some of the parameters characterizing the librational modes of the water molecules.

A similar behaviour is observed in the temperature dependence of the ammonium ν_2 mode, which is located at about 1670 cm^{-1}. Here, one also finds that the temperature dependences of the frequency, damping and strength of the bands also change at T_{c1} (figures 6(f) and (k)), while the effective mode at $\vec{E} \parallel \vec{c}$ splits into a doublet at T_{c2} (figure 6(c)).

The modes ν_1 and ν_3 of the ammonium group are located at higher frequencies (3000–3340 cm^{-1}). In this frequency range there is a strong mode mixing and an overlap of different modes and overtones. As illustrated in figures 6(h) and (m), the ν_1 mode located at 3030 cm^{-1} at room temperature shows a nearly linear increase of frequency as the temperature is lowered towards T_{c1}. However, below T_{c1} the values of $\frac{d\gamma_{TO}}{dT}$ and $\frac{d(\Delta\varepsilon)}{dT}$ are clearly modified.

In the paraelectric phase, the triplet originating from the ν_3 modes can be clearly discriminated, as expected from symmetry considerations. At T_{c1}, an additional mode appears at 3230 cm^{-1}, which likely signals the symmetry breakdown related to the onset of the first polar phase.

3.2.4. The H_2O modes. As shown in figures 7(a)–(c), the ν_1 and ν_3 modes of the water are located in the range 3300–3500 cm^{-1}. Their low dielectric strength and the partial overlap with other modes and overtones make it difficult to follow the temperature dependence of the relevant parameters quantitatively. However, figures 7(a)–(c) show that the separation in frequency of these modes exhibits a sharp increase on crossing T_{c2}. This effect suggests

that the geometry of the water molecules may be strongly modified by the second structural transformation.

More detailed information on the possible role of the H-bonds related to water molecules can be obtained from the analysis of the temperature dependence of the librational modes located in the ranges 480–520 and 680–750 cm^{-1} (figure 7). Notice that these two sets of librational modes are widely separated in frequency and display distinct selection rules (the lower frequency group is detected with the $\vec{E} \parallel \vec{a}$ or $\vec{E} \parallel \vec{c}$ geometries while the higher frequency one can be seen only for $\vec{E} \parallel \vec{b}$ or $\vec{E} \parallel \vec{c}$). This indicates that the dipolar moments associated to the two sets of modes are oriented differently with respect to the crystallographic axes. In addition, as seen in figure 7(b), one can discriminate, in the region 680–750 cm^{-1} and at $T = 250$ K, a triplet of bands for $\vec{E} \parallel \vec{b}$ that corresponds to the number of librational modes from one water molecule placed at a general symmetry site of the unit cell (factor group D_2). These results strongly suggest that the two sets of bands are due to non-equivalent molecules of water in the asymmetric unit.

The idea that two non-equivalent molecules of water in SASD give rise to libration modes located at distinct spectral regions is also supported by the analysis of the temperature dependence of the spectra. As illustrated in figures 7(d)–(g), the frequencies of both sets of bands harden, as the temperature approaches T_{c1} from above. The dielectric strength of the modes also remain practically constant as the temperature is lowered in the paraelectric phase, while the damping coefficients decrease almost linearly with temperature. However, this non-critical behaviour drastically changes at T_{c1}. Just below this temperature and as $T \rightarrow T_{c2}$, the strength and damping of the librational modes located in the higher frequency range increase (figures 7(h), (i)), while the frequency decreases (figures 7(e), (f)). This suggests that the H-bonds related to these water molecules may play an active role in the mechanisms of the second structural phase transition. In contrast, the temperature dependence of the parameters of the bands located in the range 480–520^{-1} is not affected by the first phase transition (see figure 7(d)). Moreover, while the higher frequency band detected for $\vec{E} \parallel \vec{c}$ splits at T_{c1}, the lower frequency band is only affected by the symmetry breakdown at T_{c2} (see figure 7(c)). This fact seems to indicate that the two non-equivalent water molecules are differently bonded to the crystal structure and sense the structural transformations differently. Structural studies would be highly desirable to further elucidate this point.

4. Conclusion

The data reported above unambiguously show that the temperature dependences of the frequency, damping and strength of most of the polar phonon modes change in the vicinity of the ferroelectric phase transition at $T_{c1} = 95$ K. Also, a drastic and discontinuous change of the reflectivity spectra marks the second structural transition at $T_{c2} = 79$ K.

Let us consider the first aspect. The wealth of critical anomalies detected at T_{c1} is not common in typical order–disorder transitions. In fact, because the (overdamped) critical relaxational instability is usually located at frequencies ($<10^{10}$ Hz) that are much lower than those of the phonon modes (10^{12}–10^{14} Hz), one should expect only a weak or moderate coupling between phonons and pseudo-spins, giving rise to little or more subtle spectroscopic evidence of the phase transition. The sensitivity of the lattice dynamics to the first transition indicates that below T_{c1} there exists a strong coupling between the order parameter and the phonons.

However, the data are also not typical of a displacive phase transition. In the paraelectric phase, we find no evidence of a critical soft mode, which is the expected signature of this type of transition. Actually, a closer look at the temperature dependence of the vibrational parameters

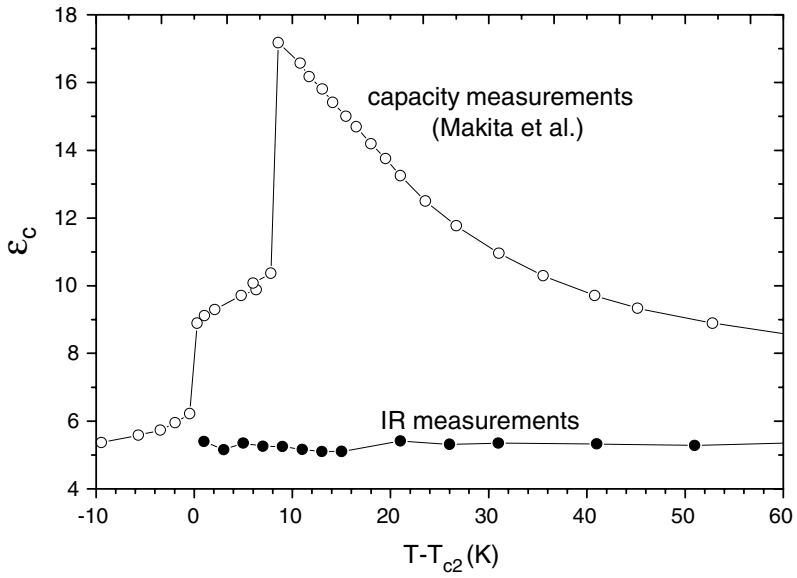

Figure 8. The dependence of ε_c on temperature deduced from capacity measurements at 10 kHz (circles; from Makita *et al* [11]) and the lattice contribution to the static dielectric constant ε_c^{phon} (dots).

in the paraelectric phase shows that there are no precursory signs of the transition. Typically, in this phase, the values of the transverse optical frequencies increase slightly as the temperature decreases while the damping decreases almost linearly. In this temperature range, the lattice dynamics show a non-critical behaviour.

Regarding this point, it is interesting to compare the temperature dependence of the low frequency dielectric constant with that of the phonon contribution to the static dielectric constant. In figure 8 we compare the dielectric constant measured along the c-axis (ε_c) at 10 kHz (data obtained from [11]) with the phonon contribution to ε_c estimated as $\varepsilon_c^{phon} = \varepsilon_{c\infty} + \sum_i \Delta\varepsilon_{ci}$, where $\Delta\varepsilon_{ci}$ represents the dielectric strength of the ith mode obtained from equation (3).

As seen, in the paraelectric phase, while the dielectric constant obtained from capacity measurements increases slightly as $T \rightarrow T_{c1}$ from above, ε_c^{phon} remains nearly independent of temperature. This means that the critical behaviour observed in ε_c in the paraelectric phase is entirely due to excitations with typical frequencies that are much lower than the phonon frequencies. Although we could not find any clear evidence of a central mode in the reflectivity spectra, this situation points to an order–disorder limit, in variance with the earlier assumption of displacive origin based on ^{23}Na magnetic resonance measurements [35].

Let us consider, as one example, the case of the internal modes of the sulfate group whose spectral signatures are depicted in figure 5. As previously stated, the correlation between T_{c1} in SASD and SASeD with the ratio of the ionic masses of SeO_4 and SO_4 points to the important role played by the SO_4 tetrahedra in the destabilization of the paraelectric phase. The rather small changes of the TO frequency of the internal modes of the sulfate group at T_{c1} suggest that the length and bond angles of the SO_4 pseudo-tetrahedra are hardly affected on crossing T_{c1}. Also, the shape of the bands is little changed on crossing T_{c1}. These results seem to indicate that this group, in the ordering process occurring at the first phase transition, acts as a quite rigid unit.

Besides the existence of a second phase transition in SASD, we also have to consider the very different values of the dielectric constant and electrical polarization observed in SASeD and SASD at the lower temperature ferroelectric phase. These facts, often overlooked in literature, suggest that different critical mechanisms may be present in the two compounds.

Let us consider first the case of SASeD. In this compound, structural, NMR and EPR data taken in the paraelectric phase show that the SeO_4 ions are in a state of rapid reorientation with respect to several axes [22, 24, 25]. Aleksandrov *et al* [22] estimated the dipole moment of this group in SASeD from the experimental atomic coordinates assuming a Se–O bond polarization of 1.8 Debye. The value thus obtained for the dipole moments of the SeO_4 pseudo-tetrahedron was too low (0.05 Debye) to account for the spontaneous ferroelectric polarization observed (2 μC cm^{-2}). That is, if the phase transition in SASeD is triggered by the ordering of the selenate groups (primary order parameter η) as is suggested by the ratio of critical temperatures in SASD and SASeD, then the transition must involve the spontaneous polarization P_c as a secondary order parameter. The condition for P_c being a possible secondary order parameter with a symmetry different from η is that at least one mixed invariant of the type $P_c\eta^p (p \geqslant 2)$, i.e. linear on P_c, is allowed by symmetry in the free energy expansion [36]. Given that the factor group of the paraelectric phase is D_2, such mixed invariants are forbidden.

However, if the primary order parameter η and P_c have the same symmetry (i.e. transform according to the same irreducible representation of D_2), then a bilinear term in η and P_c would be allowed ($\propto \eta P_c$). In such a case SASeD would be an example of a pseudo-proper ferroelectric and, because η would transform according to the irreducible representation B_1 of the group D_2, the ferroelectric phase would possess a monoclinic symmetry $P2_1$, as observed experimentally. In spite of the order–disorder nature of the primary order parameter, the spontaneous polarization could have a displacive nature and be induced essentially by lattice distortions resulting from the ordering of the SeO_4 groups (mixed or triggered type phase transition).

Following these lines, the rather low value of P_c observed in the case of SASD could be conciliated with the assumption of the same active or primary order parameter η (of an order–disorder type) if we assume a weaker coupling between η and P_c, that is, the polar lattice distortions induced by the ordering of the sulfate groups should be less important. Nevertheless, the stabilization of the first ferroelectric phase (of the monoclinic symmetry $P2_1$ if induced by η) gives rise to important changes in the lattice dynamics. These modifications, well illustrated by the modes of the water molecules or the NH_4 group (see figures 6, 7), show that a stronger coupling between pseudo-spins and phonons is established.

Our data also suggest that, in SASD, the two types of water molecule are differently bonded to the crystal network and sense the symmetry breaking induced by the ordering of the sulfate groups differently. This behaviour, which is not observed in SASeD, points to different geometries and strength of the H-bonds associated to the two non-equivalent water molecules. This difference in the bonding of the water molecules may modify the coupling between the lattice and the active SO_4 group and help explain the different values of the spontaneous polarization observed in the two compounds.

The reflectivity spectra also exhibit dramatic changes at $T_{c2} = 79$ K, which indicate that an important and discontinuous symmetry breakdown occurs at this second phase transition. The microscopic origin of this second phase transition is not well understood. Within the framework of the modified Mitsui model [23, 24], it is seen as originating from a competition between the polar order parameter and an 'anti-ferroelectric type' one, describing a competing coupling between the electric dipole momenta in each unit cell. Previous ^{23}Na magnetic resonance measurements [35] have suggested that this phase transition involved little lattice distortion. However, the magnitude of the spectral changes reported in the present work suggests that

this may not be the case. As illustrated in figures 5, 6, 7, on crossing T_{c2}, the spectral shape of the bands related to the internal modes of the water molecules and the tetrahedral groups changes profoundly. In variance with magnetic resonance data, this fact indicates that a considerable lattice distortion occurs at the second phase transition. Below T_{c2}, the value of the low frequency dielectric constant is determined only by the phonon contribution, via a Lyddanne–Sachs–Teller mechanism. Structural studies would be highly desirable to further elucidate this point and to clarify the driving mechanism of this second phase transition.

Finally, we note that, from our data, we could not find any spectroscopic evidence of a higher temperature phase transition, occurring near $T = 200$ K, whose existence has been proposed from the analysis of EPR data in Mn^{2+}-doped samples [20, 24].

References

[1] Cochran W 1959 *Phys. Rev. Lett.* **3** 412
[2] Hill R M and Ichiki S K 1963 *Phys. Rev. Lett.* **132** 1603
[3] Buixaderas E, Kamba S and Petzelt J 2004 *Ferroelectrics* **308** 131–92
[4] Merunka D and Rakvin B 2004 *Solid State Commun.* **129** 375
[5] Koval S, Kohanoff J, Migoni R L and Tosati E 2002 *Phys. Rev. Lett.* **89** 187602
[6] Sugimoto H and Ikeda S 1991 *Phys. Rev. Lett.* **67** 1306
[7] Merunka D and Rakvin B 2004 *Ferroelectrics* **319** 99
[8] Stern E A and Yacobi Y 1996 *J. Phys. Chem. Solids* **57** 1449
[9] Pérez-Mato J M, Ivantchev S, Garcia A and Etxebarria I 2000 *Ferroelectrics* **236** 93
[10] Mathias B T and Remeika J P 1956 *Phys. Rev.* **103** 262
[11] Makita Y and Sekido T 1965 *J. Phys. Soc. Japan* **20** 954
[12] Pepinsky R, Vedam R, Okaya Y and Hoshino S 1958 *Phys. Rev.* **111** 1467
[13] Jona F and Pepinsky R 1956 *Phys. Rev.* **103** 1126
[14] Godfrey L and Philip J 1996 *Phys. Rev.* B **54** 15708
[15] Baker J M, Kuriata J, O'Connel A C and Sadlowski L 1995 *J. Phys.: Condens. Matter* **7** 2321
[16] Kuriata J, Sadlowski L and Stefaniuk I 1995 *J. Phys.: Condens. Matter* **7** 2333
[17] Kuriata J, Baker J M, Sadlowski L, Stefaniuk I and Bodziony T 1998 *J. Phys.: Condens. Matter* **10** 407
[18] Lipinski I E, Kuriata J, Natkaniec I and Pawlukojc A 2001 *Phys. Status Solidi* b **299** 70
[19] Kuriata J, Lipinski I E, Korynevskii N A and Bodziony T 2001 *Physica* B **307** 203
[20] Bodziony T, Lipinski I E, Kuriata J and Bednarski W 2001 *Physica* B **299** 70
[21] Corazza E, Sabelli C and Giuseppetti G 1967 *Acta Crystallogr.* **22** 683
[22] Aleksandrov K S, Aleksandrova I P, Shabanov V F, Yuzvak V I, Nozik Y Z and Fikin L I 1978 *Phys. Status Solidi* a **45** 53
[23] Korynevskii N A 2002 *Ferroelectrics* **268** 207
[24] Lipinski I E, Korynevskii N A, Kuriata J and Pastusiak W 2003 *Physica* B **327** 116
[25] Lipinski I E, Kuriata J and Korynevskii N A 2005 *Ferroelectrics* **317** 115
[26] Mitsui T 1958 *Phys. Rev.* **111** 1259
[27] Aleksandrov K S, Aleksandrova I P, Zherebtsova L I, Rostuntseva A I, Leibivich T A and Zaitseva P 1970 *Sov. Phys.—Solid State* **11** 1639
[28] Acharya P K and Naraynan P S 1973 *Indian J. Pure Appl. Phys.* **11** 514
[29] Berreman D W and Unterwald F C 1968 *Phys. Rev.* **174** 791
[30] Farrugia L J 1997 *J. Appl. Crystallogr.* **30** 565
[31] Rousseau D L, Bauman R P and Porto S P S 1981 *J. Raman Spectrosc.* **10** 253
[32] Fawcett V, Long D A and Sankaranarayanan V N 1975 *J. Raman Spectrosc.* **3** 217
Fawcett V, Long D A and Sankaranarayanan V N 1975 *J. Raman Spectrosc.* **3** 197
[33] Wagner E L and Hornig D E 1950 *J. Chem. Phys.* **18** 305
[34] Torrie B H, Lin C C, Binbrek O S and Anderson A 1972 *J. Phys. Chem. Solids* **33** 697
[35] Genin D J and O'Reiley D E 1969 *J. Chem. Phys.* **50** 2842
[36] Tolédano J C and Tolédano P 1987 *The Landau Theory of Phase Transitions* (Singapore: World Scientific)